Influences of the Antarctic Ozone Hole on Southern Hemispheric Summer Climate Change

Citation: Bandoro, Justin, Susan Solomon, Aaron Donohoe, David W. J. Thompson, and Benjamin D. Santer. "Influences of the Antarctic Ozone Hole on Southern Hemispheric Summer Climate Change." J. Climate 27, no. 16 (August 2014): 6245–6264. © 2014 American Meteorological Society

As Published: http://dx.doi.org/10.1175/jcli-d-13-00698.1

Publisher: American Meteorological Society

Persistent URL: http://hdl.handle.net/1721.1/95750

Version: Final published version: final published article, as it appeared in a journal, conference proceedings, or other formally published context

Influences of the Antarctic Ozone Hole on Southern Hemispheric Summer Climate Change

JUSTIN BANDORO, SUSAN SOLOMON, AND AARON DONOHOE

Department of Earth, Atmospheric and Planetary Sciences, Massachusetts Institute of Technology, Cambridge, Massachusetts

DAVID W. J. THOMPSON

Department of Atmospheric Science, Colorado State University, Fort Collins, Colorado

BENJAMIN D. SANTER

Program for Climate Model Diagnosis and Intercomparison, Lawrence Livermore National Laboratory, Livermore, California

(Manuscript received 15 November 2013, in final form 16 March 2014)

ABSTRACT

Over the past three decades, Antarctic surface climate has undergone pronounced changes. Many of these changes have been linked to stratospheric ozone depletion. Here linkages between Antarctic ozone loss, the accompanying circulation changes, and summertime Southern Hemisphere (SH) midlatitude surface temperatures are explored. Long-term surface climate changes associated with ozone-driven changes in the southern annular mode (SAM) at SH midlatitudes in summer are not annular in appearance owing to differences in regional circulation and precipitation impacts. Both station and reanalysis data indicate a trend toward cooler summer temperatures over southeast and south-central Australia and inland areas of the southern tip of Africa. It is also found that since the onset of the ozone hole, there have been significant shifts in the distributions of both the seasonal mean and daily maximum summertime temperatures in the SH midlatitude regions between high and low ozone years. Unusually hot summer extremes are associated with anomalously high ozone in the previous November, including the recent very hot austral summer of 2012/13. If the relationship found in the past three decades continues to hold, the level of late springtime ozone over Antarctica has the potential to be part of a useful predictor set for the following summer's conditions. The results herein suggest that skillful predictions may be feasible for both the mean seasonal temperature and the frequency of extreme hot events in some SH midlatitude regions of Australia, Africa, and South America.

1. Introduction

In the last few decades of the twentieth century, anthropogenic halocarbon emissions have led to a dramatic decline in levels of stratospheric ozone over the Antarctic, with an ozone hole forming each year in the austral spring. The chemistry leading to the formation of the ozone hole occurs only over a limited time each year (Solomon 1999), giving the ozone loss strong seasonality. From the 1970s through the mid-2000s, recent climate change in the Southern Hemisphere (SH) has been marked by stratospheric radiative cooling from ozone depletion (Randel et al. 2009), as well by a strengthening of the westerlies and a poleward shift in the position of the jet. These changes have occurred not only in the stratosphere (Waugh and Randel 1999; Zhou et al. 2000; Thompson and Solomon 2002), but also in the troposphere (Thompson and Solomon 2002; Gillett and Thompson 2003).

Studies have proposed both dynamical (Haynes et al. 1991; Song and Robinson 2004; Thompson et al. 2006; Orr et al. 2012) and radiative (Grise et al. 2009) mechanisms to explain this deep coupling in circulation between the stratosphere and troposphere (Thompson and Wallace 2000; Jones and Widmann 2003; Thompson

Corresponding author address: Justin Bandoro, Department of Earth, Atmospheric and Planetary Sciences, Massachusetts Institute of Technology, 77 Massachusetts Avenue, Cambridge, MA 02139.
E-mail: jbandoro@mit.edu

DOI: 10.1175/JCLI-D-13-00698.1

et al. 2005), where the tropospheric response lags the springtime ozone loss and maximizes in the austral summer. Although the role of the different proposed mechanisms remain uncertain, it is clear that changes in the stratospheric polar vortex are coupled to variability in the tropospheric flow (Thompson et al. 2011; Gerber et al. 2012). As a result, the leading mode of SH extratropical variability, the Southern Hemisphere annular mode (SAM) (Kidson 1988; Karoly 1990; Hartmann and Lo 1998; Thompson and Wallace 2000), has exhibited a trend toward more positive polarity (westerly winds enhanced around 60°S and weakened around 40°S) (Hurrell and Van Loon 1994; Karoly et al. 1996; Jones and Widmann 2003; Marshall 2003, 2007; Fogt et al. 2009a). While increases in greenhouse gases (GHGs) are also expected to produce a tendency toward more positive SAM phase in all seasons (Fyfe et al. 1999; Kushner and Polvani 2004; Stone et al. 2001; Cai et al. 2003; Rauthe and Paeth 2004), the most pronounced changes in the SAM have occurred in the summer season, and are dominated by ozone loss. For example, using cluster analysis applied to reanalysis data, Lee and Feldstein (2013) identified a key role for ozone depletion in the observed shift in the SH summer jet. The interannual variations in the level of ozone depletion (i.e., the year-to-year variability with the longer-term trend removed) are due to interactions between planetary waves, the mean circulation, gravity wave drag, and the quasi-biennial oscillation (QBO) (Shindell et al. 1997), which modulate stratospheric temperatures and the strength of the polar vortex.

It is also known that the austral summer SAM is related to El Niño–Southern Oscillation (ENSO) on interannual and interdecadal time scales (Karoly 1989; Seager et al. 2003; L'Heureux and Thompson 2006; Lu et al. 2008; Chen et al. 2008), with more frequent La Niña conditions corresponding to a weakened subtropical jet and positive phase of the SAM. For this reason, the ENSO signal in surface temperatures is removed in this study when analyzing the ozone signal in surface temperatures. The relationship between ozone depletion and ENSO was also investigated in terms of the relative contributions to the long-term and interannual changes in the summer SAM.

At the surface, a summertime cooling trend over the Antarctic plateau and a warming trend over the Antarctic peninsula have been associated in part with ozone depletion and its effects on the SAM (Thompson and Solomon 2002). Several previous studies have linked both interannual and longer decadal variations in the SAM to temperature changes elsewhere in the SH (Thompson and Solomon 2002; Gillett and Thompson 2003; Gillett et al. 2006; Manatsa et al. 2013) and with cooler conditions in the summer over much of eastern Australia (Hendon et al. 2007; Meneghini 2007). More recent modeling and observational studies have shown that ozone depletion can affect both mean and extreme rainfall in the southern subtropics, with enhanced precipitation in Australia and South America in the austral summer (Kang et al. 2011; Fyfe et al. 2012; Kang et al. 2013; Gonzalez et al. 2014). The positive SAM trend reflects a poleward shift of the extratropical jet and accompanying storm tracks (Archer and Caldeira 2008) and a poleward shift of the edge of the Hadley cell (Hu and Fu 2007). It has been suggested that recent trends in the SH circulation and rainfall in austral summer are linked to stratospheric ozone depletion (Karpechko et al. 2008; Polvani et al. 2011).

A recent study by Son et al. (2013) looked at the links between September ozone concentration and both the precipitation and temperatures in the SH in the following months. These links were explored in the context of coupling with the SAM. While Son et al. found a significant correlation in the month of October over much of Antarctica and Australia, with higher (lower) levels of ozone associated with warmer (cooler) temperatures, their analysis did not find a significant link between the year-to-year variability of September ozone with the SAM index and tropospheric temperatures (at lags longer than a month). In contrast to Son et al. our focus here is not on the ozone behavior in September, but rather on the linkages between the extent of later spring November ozone loss and summertime SH midlatitude surface temperatures. We concentrate on these linkages because it is known that the ozone hole has led to an increase in incidence of high-index summer SAM (Thompson et al. 2011) and that spring total ozone is negatively correlated with the SAM at periods varying between one to four months later (Fogt et al. 2009a). While the link with interannual variations in ozone does not imply direct causality on that time scale, it will be shown that the south polar ozone is a useful measure of changes in stratospheric circulation (i.e., the polar vortex strength) and the subsequent tropospheric response.

We examine the level of ozone loss in the late austral spring month of November, the subsequent summertime SAM response, and the effects on mean and maximum temperatures in the SH midlatitudes. We focus on November because this is when the radiative perturbation from ozone maximizes in the lower stratosphere (Shindell and Schmidt 2004). Our analysis includes the recent record hot Australian summer of 2012/13. We first examine the vertical structure of December–February (DJF) long-term temperature trends to identify patterns of circulation changes that extend from the stratosphere to the troposphere. We then evaluate the extent to which the

surface tropospheric trends are congruent with the SAM. Temperature advection and potential feedbacks from precipitation changes associated with the SAM are shown to be key to understanding the spatial distribution of observed surface temperature responses. Many locations showing the strongest relationships between DJF temperatures, ozone depletion, and SAM changes are found in the dry interiors of Australia (20°–40°S) and southern Africa (poleward of about 25°S), where summer rainfall is especially important to seasonal temperature change.

Support for our findings is provided by observed differences in the relationship between ozone levels and summer temperatures (mean and extremes) before the ozone hole developed (1956–84) and in recent decades (1985–2012). As shown in model simulations by Shaw et al. (2011), the vortex breakup is delayed following the period of ozone depletion, leading to increased downward wave coupling between the stratosphere and troposphere in the SH. A related study by Manatsa et al. (2013), which focused on the climate of different parts of Africa before and after the development of the ozone hole, found significant links between the development of the Antarctic ozone hole and the surface air temperatures equatorward of 25°S. These links were more pronounced in parts of Africa in which the phase of the SAM affects the Angola low. Our study extends the Manatsa et al. analysis to the rest of the SH, using a greater number of observational datasets and longer records.

The focus of the study is on the contribution of both the longer-term ozone trend and the year-to-year variations in November ozone on the summertime temperature, atmospheric circulation, and precipitation at SH midlatitudes. We do not exclude the role of other longer-term anthropogenic climate change factors, such as increases in greenhouse gases, which have also been found to substantially influence both the mean summer temperatures in the SH (Shindell and Schmidt 2004; Kushner et al. 2001; Karoly and Wu 2005) and extreme summer temperatures in Australia (Whetton et al. 1993; Hennessy and Pittock 1995; Lewis and Karoly 2013). For example, despite the cooling trend over Australia since the onset of the ozone hole, there has been a longer-term warming trend over the twentieth century in summertime maximum temperatures across Australia (Suppiah et al. 2001).

2. Data and methods

The following is a brief summary of the analysis methods and data used. Further details are provided in the appendix.

a. Data

Because of differences in the temporal and regional availability of observational records, and to examine sensitivity to observational uncertainty, we used a variety of different datasets. To analyze changes in the vertical structure of zonal-mean monthly mean atmospheric temperatures during the period from December 1979 to February 2013, we used two reanalysis-based products: the Modern-Era Retrospective Analysis for Research and Applications (MERRA; Rienecker et al. 2011) and the Interim European Centre for Medium-Range Weather Forecasts (ECMWF) Re-Analysis (ERA-Interim; Dee et al. 2011). We also employed the gridded Hadley Centre air temperature (HadAT2) radiosonde observations (Thorne 2005). Surface temperature data were obtained from both ERA-Interim and station observations from version 3.2.0 of the National Climatic Data Center's Global Historical Climatology Network (GHCN) (Lawrimore et al. 2011). Our analysis of observed changes in monthly mean precipitation relied on results from version 2.1 of the Global Precipitation Climatology Project (GPCP) (Adler et al. 2003), which is a gridded product based on observations from both rain gauge stations and satellite instruments. Ground-based total column ozone measurements from the Halley Station (72°S, 27°W), which has been in near-continuous operation since 1956, were obtained from the Reference Antarctic Data for Environmental Research (READER; Turner et al. 2004). To investigate the effects of ozone depletion on SH mean and maximum daily temperatures, data were obtained from both the Australian Climate Observations Reference Network–Surface Air Temperature (ACORN-SAT; Trewin 2013) and GHCN. When analyses were performed for individual countries, only countries with at least three stations with continuous data measurements were considered. In addition to Australia, these include Botswana, Namibia, South Africa, and Argentina. The index used for the regression-based removal of ENSO effects is the record of sea surface temperatures anomalies in the Niño-3.4 region (5°S–5°N, 170°–120°W) from the National Weather Service Climate Prediction Center (http://www.cpc.ncep.noaa.gov/data/indices/ersst3b.nino.mth.ascii). By convention in this study, the corresponding year associated with the DJF season is the year with the month of December.

The reliability of multidecadal temperature and circulation trends estimated from reanalysis products can be affected by inhomogenities in the assimilated data, by spatial and temporal changes in data coverage, and biases in the assimilation model (Santer et al. 1999; Trenberth et al. 2011; Bosilovich et al. 2011). We therefore focus on trends calculated over the satellite era, a period that did

not involve large changes in the coverage or ''mix'' of assimilated data. Our use of multiple reanalyses (in conjunction with radiosonde and/or surface station measurements) helps us to evaluate the sensitivity of our findings to current uncertainties in reanalysis products and observations.

b. Analysis

1) Regressions and congruence

Here, we calculate least squares linear trends of monthly anomalies. The method used to determine statistical significance of trends is described in the appendix. Regression coefficients and congruence between two time series are obtained using detrended anomalies, following the approach in Thompson and Solomon (2002). The SAM congruent trend found by application of this method, however, may not represent the true long-term response to decadal changes in SAM, particularly at higher latitudes (see Sigmond et al. 2010; Bitz and Polvani 2012; Smith et al. 2012). This is due to two different response time scales of the Southern Ocean to the SAM. The first is an Ekman-induced fast cooling period in response to the positive SAM phase around Antarctica, followed by a slower ocean eddy-diffusive-driven multidecadal warming response from ozone-induced strengthening of high-latitude westerlies (Fyfe et al. 2007; Screen et al. 2009; Marshall et al. 2014). Surface effects from the opposing interannual and long-term changes are largely restricted to those located in the high-latitude Southern Ocean and are less important to the subpolar regions that are the primary focus of this study.

2) SAM index

The DJF SAM index used in this study was developed by Marshall (2003), based on the definition of Gong and Wang (1999). The index is simply the difference in normalized mean zonal pressure at 40° and 65°S (http://www.antarctica.ac.uk/met/gjma/sam.html). The results presented in this analysis were insensitive to whether we used this definition of the SAM or that based on the leading principal component analysis (e.g., Thompson and Wallace 2000) of reanalysis-based geopotential height data poleward of 20°S.

3) Removal of the ENSO signal

To determine the link between summer surface temperatures and the previous springtime Antarctic ozone levels, it is helpful to remove other known sources of interannual variability that might mask or mimic the signal. One important source of such variability is ENSO, which has teleconnections with weather anomalies in extratropical latitudes. Lagged correlation coefficients were calculated between the detrended time series of the monthly ENSO index and the gridded temperature data. Using the optimal lag (in months) that maximizes the regression coefficient, the time series of interest was then regressed against the ENSO index. We discuss below several tests in which the ENSO signal was removed in this manner prior to analysis of ozone depletion signals.

4) Probability distributions of maximum daily temperatures

We also consider surface daily maximum temperatures, and how these temperatures have changed in pre–ozone hole and ozone hole eras. We test whether the distributions of daily maximum temperatures in high and low ozone years prior to and after the formation of the ozone hole are significantly different from each other. In the ozone hole era, the null hypothesis is that in a number of different regions of the SH, years with high ozone have no shift or changes in distribution of the frequency of hot summer events when compared to years with anomalously low ozone (see the appendix for details of how distributions were calculated).

For Australian stations, observations beginning in 1950 through 2013 were sorted into five climatologically distinct regions outlined by the Australian Bureau of Meteorology: northern, southern, southwestern, southeastern, and eastern Australia. For other countries in the SH, all available station observations reported in the GHCN were used. We applied Kolmogorov–Smirnov and Mann–Whitney tests to determine whether the distributions of summertime maximum surface temperature in years with anomalously high and low ozone were significantly different in both pre–ozone hole and ozone hole periods [see Lehmann (2006) for details of the tests].

3. Results

a. SH summer temperature trends (1979–2012)

Figure 1 shows the zonally averaged vertical structure of the trend in temperature in DJF from the two reanalyses and the HadAT2 radiosonde dataset. Surface pressure data for the reanalysis-based estimates was used to mask out the topography over Antarctica. Removal of the ENSO signal did not have a significant effect on the estimated zonal-mean vertical trends. There are two key features common to all datasets: the first is the midtropospheric summer warming in the midlatitudes flanking the extratropical jet, which is consistent with the dynamic signature of a trend toward a more positive SAM, and the second is the cooling over the Antarctic continent in the troposphere. Both

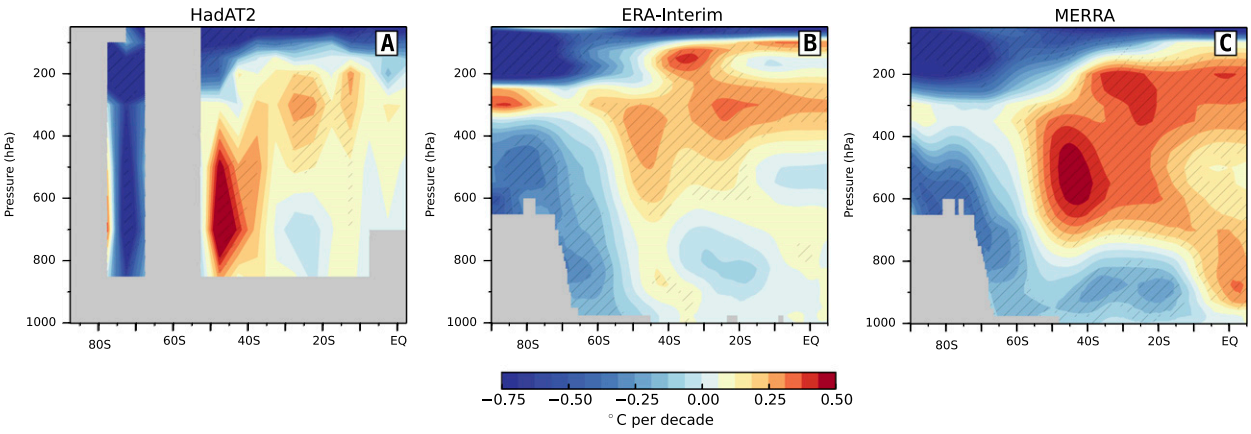

FIG. 1. Zonal mean linear trend in DJF seasonal mean atmospheric temperatures over 1979 to 2012. Results are for the (a) HadAT2 radiosonde archive, (b) ERA-Interim reanalysis, and (c) MERRA reanalysis. Hatching indicates regions significant at the 10% level, estimated using a two-sided Student's *t* test (see the appendix). Gray regions denote missing data in HadAT2, and areas below the material surface in the reanalyses.

are driven by vertical motion induced by anomalous northward momentum fluxes: rising air over the pole drives adiabatic cooling; sinking air in the midlatitudes drives adiabatic warming (Orr et al. 2012). The strong high-latitude cooling in the lower stratosphere is the direct radiative signature from the long-term ozone depletion.

In the midlatitudes, however, warming is not coherent through the full depth of the troposphere. Both reanalyses show reduced midlatitude warming (or even slight cooling). The HadAT2 radiosonde data show similar structure, but the magnitude of the changes in HadAT2 are larger than the reanalysis, most likely due to the relatively limited spatial coverage. The maximum warming feature in HadAT2 is displaced closer to the surface, which may reflect its coarser vertical resolution (9 levels, compared to 42 and 46 levels for ERA-Interim and MERRA, respectively).

This feature is investigated in the remainder of this section. We will show that surface temperature changes are strongly influenced by changes in horizontal temperature advection and potential feedback mechanisms such as precipitation. Although the vertical temperature patterns mentioned above are similar among the datasets, they differ in both magnitude and sign in the tropical free atmosphere and in the sign of zonal-mean trends near the surface even between reanalysis products. The differences with the radiosonde dataset observations may reflect the spareness of measurements in both space and time in the SH, while the differences in reanalyses may be due to differences in data assimilation.

To investigate physical links between the polar stratosphere and the midtropospheric warming near 40°S (see Figs. 1a–c), we compare time series of total column ozone with various indices of stratospheric and tropospheric circulation (see Fig. 2). The radiative temperature response to ozone depletion has been shown to affect circulation in the polar stratosphere (Gillett and Thompson 2003; Perlwitz et al. 2008; Haigh and Roscoe 2009; Thompson et al. 2011) and is thought to be the primary driver of the long-term change in the summer SAM. On shorter time scales, interannual variations in the strength of the wintertime polar stratospheric vortex are strongly influenced by the flux of planetary wave activity from below (Matsuno 1971; Schoeberl and Hartmann 1991; Christiansen 1999; Hartmann et al. 2000; Polvani and Waugh 2004; Gerber et al. 2012). In the SH, studies by Polvani and Waugh (2004) and Fogt et al. (2009b) found that winter and early spring stratospheric wave driving is significantly correlated with the summer SAM, suggesting a relationship between the wave driving and SAM on interannual time scales. In winter and early spring, anomalously strong upward fluxes of wave activity into the stratosphere are associated with both a weaker stratospheric vortex and increased transport of ozone into the vortex (stronger Brewer–Dobson circulation and potential vorticity stirring in the surf zone) and a subsequent weaker summer SAM by downward influences (Thompson et al. 2006; Chen et al. 2008). Thus, year-to-year perturbations of stratospheric wave activity can affect not only the interannual variations in the summer SAM but also the year-to-year ozone concentrations (Li et al. 2010), which in turn can influence the lower stratospheric circulation and affect the summer SAM, and hence can influence the tropospheric circulation through radiative processes (Grise et al. 2009). The complex spatially and temporally varying interactions of wave activity, total column

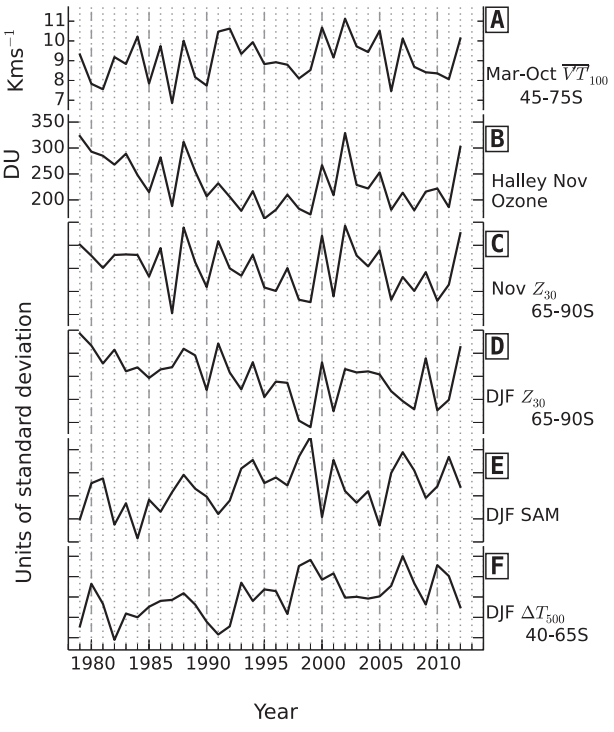

FIG. 2. Time series of (a) extratropical southward eddy heat flux at 100 hPa from ERA-Interim, time averaged from March to October and spatially averaged (with area weighting) over 45°–75°S, derived from ERA-Interim; (b) November total column ozone from the Halley station; (c) standardized geopotential height anomalies in November at 30 hPa; and (d) as in (c), but for DJF. Both (c) and (d) are area weighted averages over the pole (65°–90°S) and are calculated from ERA-Interim. Also shown are (e) the Marshall (2003) DJF SAM index and (f) the ERA-Interim anomalies of the temperature gradient between the latitudes of 40° and 65°S at 500 hPa.

ozone, and interannual variations of summertime tropospheric circulation are not fully understood, and the influence of ozone losses, in addition to wave driving, on interannual changes in SAM cannot be ruled out.

Figure 2a shows the time series of the wintertime vertical Eliassen–Palm (EP) flux at 100 hPa. Results are cosine-weighted over 45° to 75°S from March to October, as in Weber et al. (2011), and are estimated as the zonal-mean northward eddy heat flux, $\overline{V'T'}$, representing the vertical transmission of momentum by tropospheric planetary waves (Andrews et al. 1987; Salby 2008). Here the 6-hourly zonal-mean anomalies of temperature and meridional wind from ERA-Interim were used for computing the vertical EP flux. Underneath in Fig. 2b is the November total column ozone from the Halley station. It can be seen that years with anomalously high wintertime EP flux are associated with higher springtime levels of ozone. The time series of cosine-weighted zonal-mean 30-hPa geopotential height anomalies over the South Pole are plotted in Figs. 2c and 2d for November and December–February (respectively). These months were chosen to illuminate the link between changes in wintertime wave driving, springtime ozone, and circulation changes in late spring and the subsequent peak tropospheric in the summer (Thompson and Solomon 2002). We also show the link between circulation and temperature changes in the troposphere, using the DJF SAM index and the time series of the DJF temperature gradient (between 40° and 65°S) at 500 hPa. The matrix of correlations between all detrended time series in Fig. 2 is given in Table 1.

These results suggest links among November ozone total column ozone, wintertime upward wave driving of the stratosphere, and springtime changes in circulation in the lower stratosphere. These circulation changes last until the summer, and affect both the circulation and the temperatures in the SH troposphere. This is shown by the high correlations between November ozone and changes in the 30-hPa geopotential height both in November (0.83) and in DJF (0.66). Significant correlations were also found between the southward eddy heat flux and the same two indices of stratospheric circulation changes (0.71 and 0.41, respectively). These results indicate that both stratospheric wave driving and springtime ozone are linked to interannual changes in the strength of the polar vortex.

Significant correlations are not restricted to stratospheric indices. We also find significant negative correlations of ozone (−0.39) and wave driving (−0.43) with the DJF SAM. Anomalously high (low) upward wave activity and levels of ozone are associated with a weaker (stronger) than normal stratospheric polar vortex in the spring in concert with a low (high) SAM phase in the following summer. In contrast to the results of Son et al. (2013), we find significant correlations between the detrended springtime ozone and the summer SAM when using the November total column ozone measurements.

We next examine how the spatial patterns of SH surface temperatures have changed, with a focus on the midlatitude surface cooling in Fig. 1. The spatial patterns of the 500-hPa and surface temperature trends over the 34-yr period from 1979 to 2012 are shown in Fig. 3, along with the trend that is congruent with the SAM. As noted earlier, this may not fully capture the long-term SAM forcing over the Southern Ocean and high-latitude landmasses. Surface trends are from both ERA-Interim and surface stations. In the latter case, results are overlaid with the ERA-Interim 34-yr trend in 925-hPa winds.

A prominent feature of temperature trends in the midtroposphere is the strong, zonally symmetric warming centered at around 40°S (see Fig. 1). This pattern is

TABLE 1. Correlation coefficients for the detrended time series shown in Fig. 2. Italicized and bold values are significant at the 10% and 5% levels respectively.

	Mar–Oct	Nov	Nov	DJF	DJF
	$\overline{V'T'}_{100}$ (45°–75°S)	Halley O_3	Z_{30} (65°–90°S)	Z_{30} (65°–90°S)	SAM
Nov Halley O_3	**0.49**				
Nov Z_{30} (65°–90°S)	**0.77**	**0.83**			
DJF Z_{30} (65°–90°S)	**0.41**	**0.66**	**0.76**		
DJF SAM	**−0.43**	**−0.39**	**−0.49**	**−0.55**	
DJF ΔT_{500} (40°–65°S)	*−0.25*	*−0.23*	**−0.42**	**−0.61**	**0.66**

primarily dictated by changes in the annular pattern of the SAM. At the surface, the well-documented cooling over most of Antarctica is apparent in both reanalysis and surface station observations, with the SAM accounting for a large portion of the trend over Antarctica. Gillett and Thompson (2003) state that the cooling is consistent with adiabatic changes in temperature driven by thermally indirect rising motion there. The contrasting warming of the Antarctic peninsula has been documented in prior studies and linked to changes in blocking (Orr et al. 2004) and warm air advection from the Southern Ocean (Marshall 2007).

A key result, which we probe further below, relates to the trends outside of the polar regions (Figs. 3c,d), where the magnitude of the cooling is as large as over Antarctica, particularly in parts of eastern Australia.

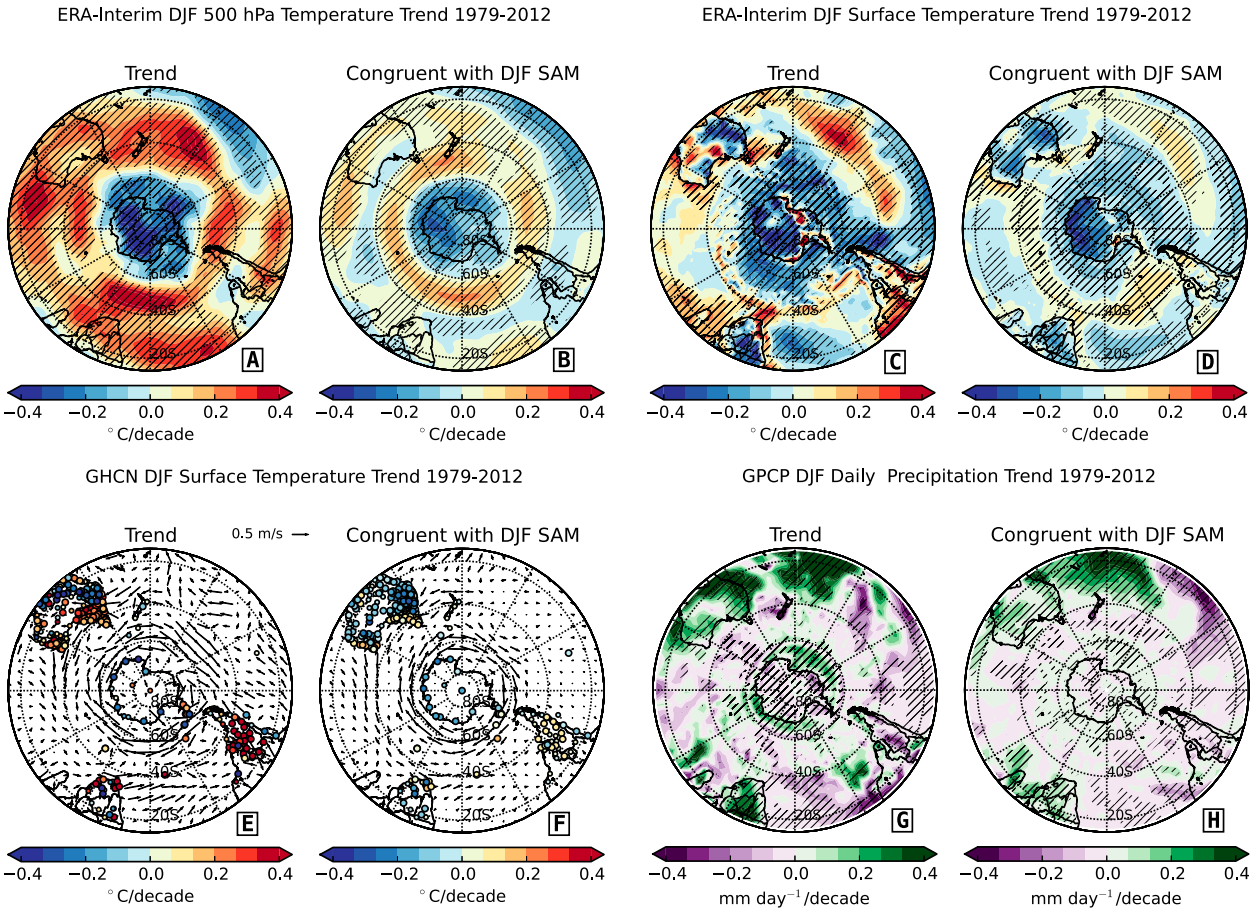

FIG. 3. (left) Summertime (DJF) temperature trends over 1979 to 2012 for (a) ERA-Interim at 500 hPa, (c) ERA-Interim at the surface, and (e) GHCN surface stations (the latter is overlaid with the total change in the ERA-Interim 925-hPa winds over the same time period), and (g) DJF trends in precipitation derived from GPCP data. (right) The adjacent panels for each trend plot [i.e., (b),(d),(f), and (h)] show the trend that is congruent with the DJF SAM. Hatching and larger filled circles indicate results are significant at the 10% level or better (estimated with a two-sided Student's *t* test).

Figures 3c–e show that this summertime cooling can be partly attributed to the trend toward higher polarity in the SAM, which causes anomalous easterly flow from the Tasman Sea and hence increased precipitation (Hendon et al. 2007) and cloud cover (Watterson 2000; Sen Gupta and England 2006). In contrast, the western coastal regions of Australia have experienced reduced westerly advection, reducing the maritime influence and resulting in dryer and warmer conditions. Trends in daily precipitation estimated from GPCP (see Fig. 3) are consistent with patterns of surface temperature changes. Our results confirm past studies indicating that the above-described trends in surface temperature and precipitation are primarily driven by changes in circulation and cloudiness. The same relationships hold not only in Australia, but also in interior and coastal regions of southern Africa. The patterns of temperature and precipitation trends are similar to those obtained by taking the difference between composites of high and low SAM index years (not shown), providing further evidence that the trends are primarily driven by the trend in the SAM.

In certain areas, however, the temperature trend congruent with the SAM does not fully capture the observed trend behavior. This is the case, for example, with the pronounced warming on the eastern side of the Antarctic peninsula, where the warming trend congruent with the SAM is not as large as observations. Similar results have been obtained by other investigators (Schneider et al. 2012; Roscoe et al. 2006; Marshall 2007). The Southern Ocean exhibits an annular warming that is stronger than the SAM-congruent trend, which may be due to the longer time scale response of the ocean to SAM forcing (as discussed earlier).

When a large number of statistical significance tests are performed, a fraction of the total number of tests are expected to yield significant results by chance alone. Another important issue is the spatial autocorrelation structure of the underlying data being tested. To assess the overall statistical significance of our results, we applied a field significance test to the individual station results in Fig. 3f. We used the method outlined by Livezey and Chen (1983). We preserved the spatial autocorrelation structure of the station temperature data, but randomly reordered the DJF SAM index 10^5 times. This allowed us to determine the fraction of stations for which the null hypothesis (no SAM congruent trend except by chance) could be rejected. Using a local significance level of $\alpha = 0.05$, the number of stations with locally significant regressions at this level that could have occurred by chance alone was calculated for each random permutation of the SAM index. Results were judged to be field significant if the total number of observed stations with locally significant regression coefficients exceeded the critical $1 - \alpha$ percentile (i.e., the top 5%) of the distribution of the total number of significant correlations obtained with randomized SAM data.

For our observed surface station temperature data, the SAM had significant association with local temperature at 59% of the 403 stations. In contrast, in the top 5th percentile of the tests conducted with the randomized SAM index, only 15% of the total number of tests yielded locally significant results. This finding implies that the SAM is having a highly significant overall impact on surface temperature at the 403 stations analyzed here. The overall field significance was not affected by the exclusion of Antarctic stations.

The annular structure of circulation changes associated with the SAM has a zonally inhomogenous impact on summertime surface temperatures in the subtropics (Figs. 3c,d) similar to the results of Gillett et al. (2006) and Hendon et al. (2007). While the forcing is indeed annular (as is evident from the circulation aloft), the nonannular surface response in these dry regions is modulated by changes in zonal advection of maritime air over the continent, and by such factors as precipitation, contrast in land–ocean heat capacity, soil moisture, and cloudiness. Differences in evaporation between land and ocean could also contribute to the differences in land–ocean temperature responses to the forcing (Joshi et al. 2008).

To further investigate whether ozone depletion can be linked to the year-to-year variability in surface temperature anomalies in SH regions outside of the South Pole, Figs. 4a and 4b show the Pearson correlation coefficients calculated for the detrended time series of November total column ozone (from Halley station) and the DJF surface air temperatures (from ERA-Interim and surface station observations). The analysis is over the period from 1979 to 2012. Large correlations are obtained not only over most of Antarctica, but also over many subpolar regions, such as southeastern Australia. The region with correlations significant at the 5% level is shown in the expanded view of Australia (Fig. 4c), and it encompasses areas where the majority of the population resides. Figure 4c also displays the correlations between the November ozone and the near-surface wind anomalies from ERA-Interim. The correlation coefficients were calculated for both the zonal and meridional wind components, and then plotted as vectors. Anomalously high spring ozone is linked to anomalous easterly winds over the eastern coast, carrying the maritime air into the interior of the continent, consistent with the link to the SAM.

The insets of Figs. 4d and 4e show the surface temperature time series for two Australian stations, Charleville and Cobar, where the summer temperatures

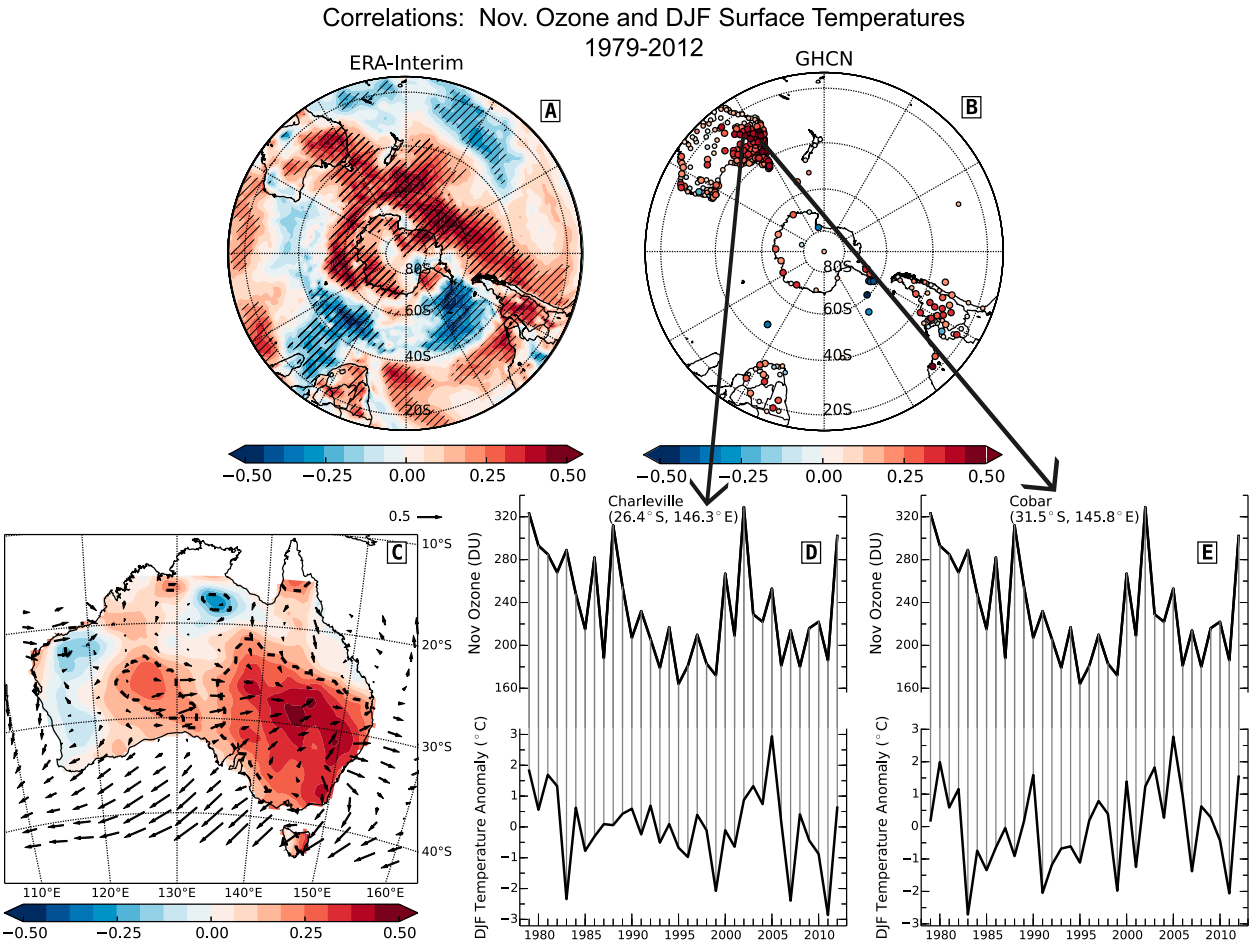

FIG. 4. Correlations between detrended summertime surface temperatures and November total column ozone from the Halley station for (a) ERA-Interim reanalysis and (b) GHCN surface station measurements. Also shown are (c) an expanded view of Australia, with the November ozone correlations and (overlaid) the 925-hPa wind-field correlations with the vector scale indicated in the top right, and the time series of ozone for two stations: (d) Charleville and (e) Cobar. Hatching in (a) and green contouring in (c) denote regions where the correlations are significant at the 5% level or better.

are significantly correlated at the 5% level (0.36 and 0.35 respectively) with the variations in total column ozone at the Halley station. Parts of southern Africa and the southern tip of South America are also significantly correlated with the interannual variations in ozone. Figure 4 shows that the Antarctic ozone hole of 2012 was among the smallest in the past 20 years, and that ozone quickly recovered to nearly pre–ozone hole values by November of that year. Consistent with this relationship, the following summer (2012/13) was anomalously warm for many Australian stations, although other factors, including greenhouse gas–driven climate change, were likely contributing factors (Lewis and Karoly 2013).

The appendix contains an additional multiple linear regression-based framework to address both the relative long-term and short-term ozone and ENSO links with the DJF SAM. It was found that both the observed trends and year-to-year variability in the summer SAM are more strongly linked in part to observations of the depth of the springtime Antarctic ozone hole than the ENSO phase. Below, we will stratify the correlations in Fig. 4 by examining periods with and without the ozone hole present. We also investigate whether ENSO has a significant influence on the size and spatial structure of the ozone and surface temperature correlations.

b. SH midlatitude summer link to springtime ozone

In this section, we stratify relationships identified in the previous section between the Antarctic ozone hole and the surface mean and daily maximum temperatures in SH midlatitude regions. Stratification is for the pre–ozone hole period and the ozone hole era. We analyze these relationships over a number of different regions of

TABLE 2. Temporal variance explained by ENSO for monthly surface temperature anomalies, displayed as the square root of the coefficient of determination. Results are grouped in the indicated regions for the four seasons in the two different eras. For Australia the different regions are as follows: E–eastern, SE–southeastern, N–northern, S–southern, and SW–southwestern.

		Australia								
Season	All	E	SE	N	S	SW	Argentina	South Africa	Namibia	Botswana
1956–84										
Summer	0.47	0.25	0.43	0.42	0.28	0.22	0.26	—	—	—
Autumn	0.38	0.30	0.45	0.15	0.41	0.11	0.24	—	—	—
Winter	0.18	0.23	0.30	0.14	0.21	0.12	0.10	—	—	—
Spring	0.29	0.37	0.25	0.29	0.25	0.30	0.04	—	—	—
1985–2013										
Summer	0.34	0.36	0.24	0.25	0.15	0.03	0.31	0.33	0.39	0.42
Autumn	0.35	0.39	011	0.10	0.46	0.10	0.15	0.22	0.50	0.51
Winter	0.21	0.16	0.10	0.10	0.25	0.09	0.12	0.11	0.11	0.03
Spring	0.16	0.03	0.19	0.19	0.13	0.16	0.10	0.15	0.09	0.10

the Australian continent, as well as over the southern tip of Africa and South America.

Table 2 shows (stratified by ozone hole and pre–ozone hole periods) the variance of monthly-mean surface temperature anomalies that can be explained by ENSO. Results are for each of the four seasons, for five regions of Australia, and for several countries in the southern tips of Africa and South America. For countries where continuous observations back to 1956 are not available, only the analysis of the ozone hole era is presented. In all seasons and regions, ENSO explains less than 25% of the temporal variance of surface temperatures, but is still significant in some seasons, with the correlation coefficient generally higher in summer. It is the summer correlation values that will be later compared to the predictability of November ozone. To facilitate the analysis of the summer temperatures link to the springtime ozone level, we first remove the ENSO signal.

Table 3 shows correlation coefficients between the detrended DJF seasonal-mean surface temperature anomalies and November ozone. Results are stratified according to the two different analysis periods, and are given with and without removal of the ENSO signal. Correlations with the previous spring's total column ozone are only statistically significant during the ozone hole era in both eastern and southeastern Australia, as well as Argentina (see corresponding Fig. 5). Table 3 also shows results of statistical testing, using the Fisher Z transform (Papoulis 1990), for whether the calculated correlations for the ozone hole era are significantly greater than those in the pre–ozone hole era. As expected from Fig. 4c, correlations are largest for eastern Australia, and parts of southern Africa and South America. In some cases, correlations are large, or even larger than those obtained for summer temperatures and ENSO (Table 2). This suggests that changes in stratospheric circulation, diagnosed by the seasonal ozone loss, are large enough to perturb the SAM and affect surface temperatures over large midlatitude regions of the SH, particularly the inland areas off the eastern coasts that are affected by changes in circulation associated with the SAM.

TABLE 3. Pearson correlation coefficients for November ozone and the summertime surface temperature anomalies in the pre–ozone hole and ozone hole eras, without and with the ENSO signal removed. Italicized and bold values indicate significance at the 10% and 5% level respectively. One and two asterisks (* and **) denote whether the correlations in the ozone hole era are significantly greater than the values in the pre–ozone hole era at levels of 10% and 5% respectively.

		Australia								
Season	All	E	SE	N	S	SW	Argentina	South Africa	Namibia	Botswana
Original										
1956–84	0.08	−0.18	−0.18	0.08	0.06	0.24	−0.06	—	—	—
1985–2012	*0.34*	**0.43** **	0.23 *	0.27	0.26	−0.02	**0.38** **	*0.35*	0.26	**0.41**
No ENSO										
1956–84	0.21	−0.03	−0.17	0.14	0.14	0.26	−0.07	—	—	—
1985–2012	*0.34*	**0.45** **	0.23 *	*0.31*	0.25	−0.02	**0.39** **	**0.36**	0.28	**0.49**

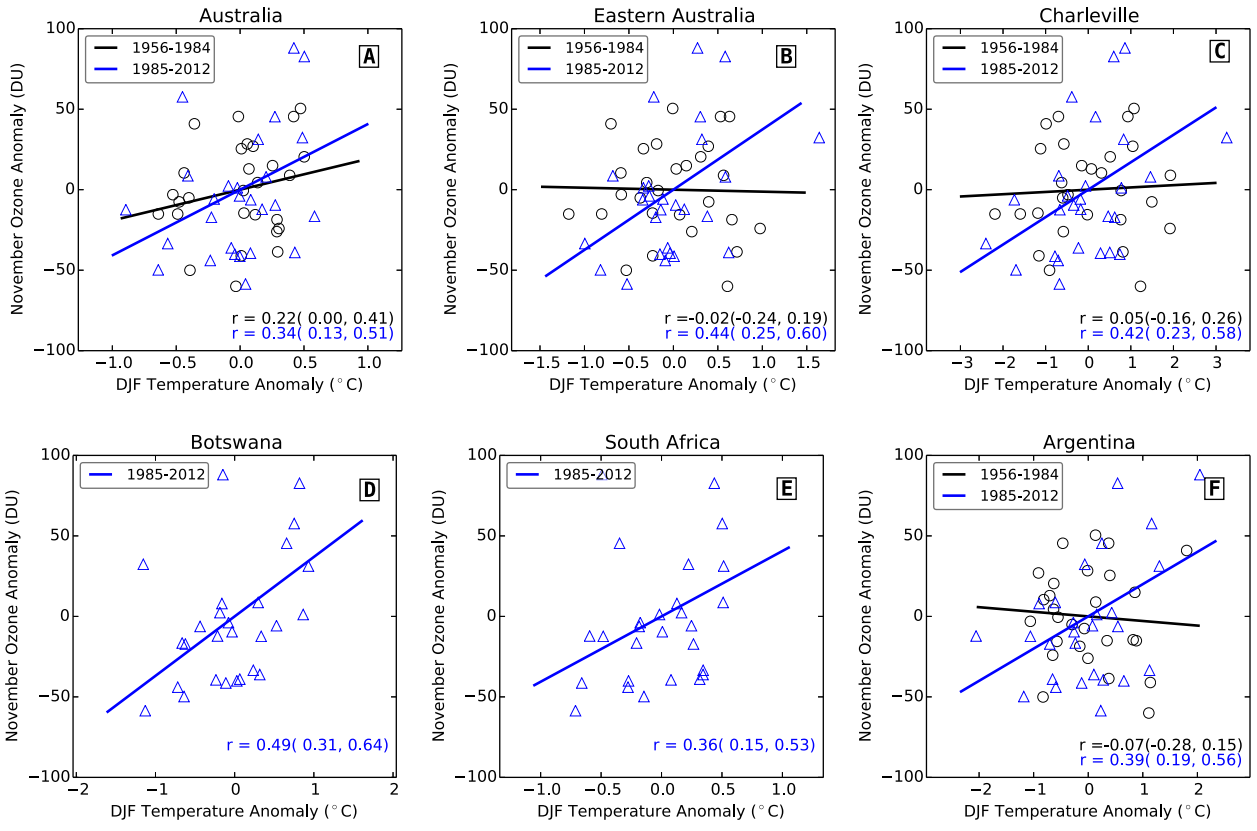

FIG. 5. Scatterplots of the November total column ozone anomalies vs DJF surface temperature anomalies for the two different eras. Results are for (a) Australia, (b) eastern Australia, (c) Charleville, (d) Botswana, (e) South Africa, and (f) Argentina. The correlation coefficients are shown with the respective 95% confidence intervals from the *F* distribution. The results displayed are for the case with the ENSO influence removed.

Figure 6 shows the distribution of daily summertime maximum temperatures in high and low ozone years in the two analysis periods. As the high and low ozone years are based on anomalies relative to the long-term trend in each period, they are not grouped at the start and end of the periods. The standard deviations for the distributions (see Table A2 in the appendix) have not changed between the two periods. In the ozone hole era, however, the distribution for high ozone years is shifted toward higher daily maximum temperatures and thus more frequent warm events, particularly for eastern Australia and Argentina. The ozone hole era data for Botswana and Namibia (Fig. 6f) show a similar shift in daily summertime maximum temperatures when comparing high and low ozone years. The shift in the distributions is visually obvious at many individual stations in these regions, such as Charleville in eastern Australia (see Fig. 6c). As noted by Lewis and Karoly (2013), these regions of Australia are particularly susceptible to bushfires in extreme summer heat. Certain species are also vulnerable to extreme heat, such as the Australian fruit bat (Welbergen et al. 2008). Extreme heat events can also negatively affect the agricultural industry (Anderson 1979; Gunasekera et al. 2008).

Following a similar analysis to that of Thompson and Wallace (2001), we investigated the frequency of the occurrence of extreme summer temperatures at stations for which the distributions between the high ozone years and low ozone years in the ozone hole era were statistically different. The results are presented in Table 4 for the stations in eastern Australia, southern Africa, and Argentina. An extreme event occurs when the daily maximum temperature exceeds a threshold of 1.5 standard deviations above the summer seasonal mean of the daily maximum temperatures (calculated over all years in ozone hole era). In all of the stations listed, the frequency of hot events increases in summers following anomalously high springtime ozone over the Antarctic. These findings suggest the springtime ozone levels could in part be a useful predictor for determining whether the following summer will be anomalously hot or cold in the regions where there are statistically significant correlations between changes in springtime SH polar ozone and summertime surface temperature (see Fig. 4b).

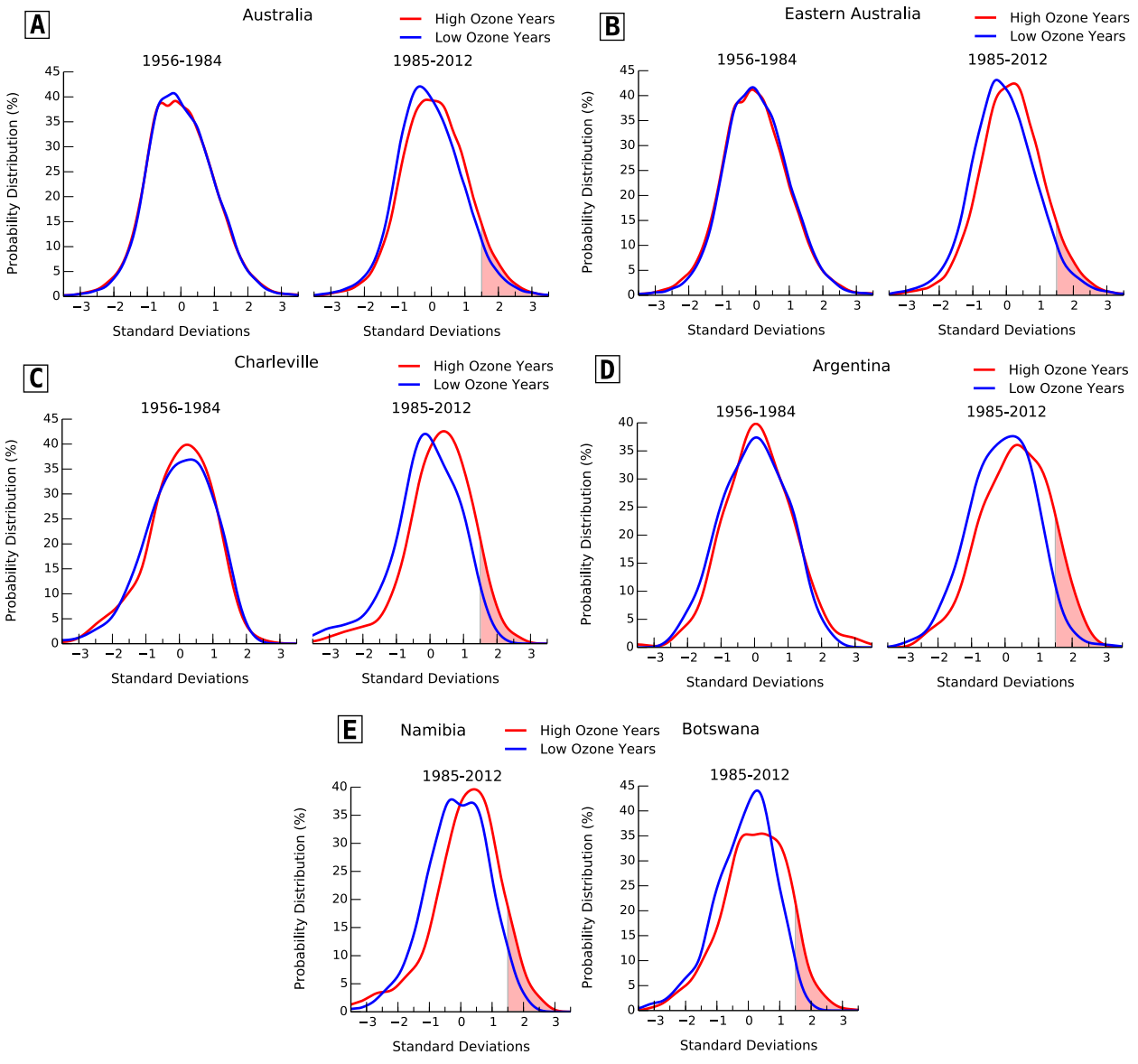

FIG. 6. Probability distribution functions of daily maximum temperatures for low and high ozone years for the two different eras analyzed for (a) Australia, (b) eastern Australia, (c) Charleville station, and (d) Argentina. (e) The same distributions are shown for Namibia and Botswana, but only for the ozone hole era, due to limited data availability. Light red shading indicates when the threshold of 1.5 standard deviations was exceeded. Table A2 in the appendix shows the value for the corresponding standard deviations along with statistical results for the other regions not shown here. Refer to the appendix for full details regarding construction of the PDFs. For the Charleville station, one standard deviation corresponds to 3.8°C in both eras.

4. Conclusions

We have shown that observations of late springtime Antarctic ozone are linked in part to lower stratospheric circulation changes and also summertime tropospheric circulation changes in terms of the SAM on both interannual and decadal time scales. While our results do not imply direct causality (since other factors, such as wintertime wave activity, also affect interannual variations in ozone and the DJF SAM), they suggest that tracking the level of springtime ozone depletion could improve predictions of summertime surface temperatures in many midlatitude regions of the SH. In the decades since the initial identification of the ozone hole, anomalously high and low spring ozone are significantly correlated with hotter and colder than normal summers over large regions of the SH, and in particular over Australia. We have shown that these relationships emerged after the mid-1980s. Our findings are consistent with the results of Shaw et al. (2011), who noted that the ozone hole acts to

TABLE 4. Frequency of events with extreme summer heat in the years following high and low Antarctic spring total column ozone between 1985 and 2012. Results are given as the percentage of days during the summer when the daily maximum temperatures exceeded the threshold indicated in the left column, which was chosen to be 1.5 standard deviations above the DJF seasonal mean over the period. Station data for the Australian stations were obtained from the ACORN-SAT database. Results from non-Australian stations were from the GHCN daily database.

Summer event and location	Frequency of occurrence (%) following:	
	High spring O_3	Low spring O_3
>40.6°C in Charleville, Australia (26.4°S, 146.3°E)	5.1	2.7
>42.5°C in Bourke, Australia (30.1°S, 135.6°E)	8.0	2.7
>40.7°C in Cobar, Australia (31.5°S, 145.8°E)	9.8	3.1
>38.2°C in Wagga Wagga, Australia (35.5°S, 147.5°E)	10.0	6.6
>38.8°C in Bloemfontein, South Africa (29.1°S, 26.1°E)	7.0	2.6
>37.8°C in Maun, Botswana (20.0°S, 23.3°E)	7.3	1.0
>35.0°C in Córdoba, Argentina (31.3°S, 64.1°W)	8.0	4.1

extend the lifetime of the polar vortex, leading to an increased coupling between the stratosphere and troposphere in the SH, and consequently the summertime SAM. Changes in circulation in the lower stratosphere associated with the level of ozone depletion propagate downward to the surface, and partially determine the surface climate response. During low (high) spring ozone years, changes in surface winds toward more easterly (westerly) flow result in an increase (decrease) in precipitation, and contribute to cooler (warmer) summertime temperatures over eastern Australia. Qualitatively similar patterns are observed over southern Africa and South America. Incidences of hot summer events in these regions were shown to also be associated with the level of ozone in the previous spring.

This work suggests that the depletion of Antarctic ozone since has acted to possibly offset a substantial portion of the summer warming that would have been caused by the increases in greenhouse gases over the past three decades. Future observations and related research will shed light on the robustness of our findings. In the next several decades the ozone hole is expected to slowly recover, but to display levels still well below the pre–ozone hole era. This recovery should help to quantify the relative contributions of changes in well-mixed greenhouse gases (Lewis and Karoly 2013) and springtime total column ozone levels to changes in the incidence of extremely hot summers. The results presented here suggest that such investigations should focus on regions with statistically significant correlations between springtime ozone and summertime surface temperature.

Acknowledgments. We would like to acknowledge and thank the following centers and agencies for access to and use of their datasets in this study: the NASA Global Modeling and Assimilation Office (GMAO), the European Centre for Medium-Range Weather Forecasts (ECMWF), the Scientific Committee on Antarctic Research (SCAR), the National Climatic Data Center (NCDC), the Met Office Hadley Centre, the Australian Bureau of Meteorology, and the Global Energy and Water Exchanges Project. JB and SS obtained partial support from an NSF FESD project on the impact of the ozone hole on the Southern Hemisphere climate and an NSERC postgraduate scholarship.

APPENDIX

Statistical Analysis and SAM Regression

a. Significance of regression analysis

We used the method outlined by Trenberth (1984) to determine the statistical significance of the least squares linear trends calculated here. This method accounts for the effects of autocorrelation by calculating the number of effectively independent samples for use in the Student's t test of the statistical significance of the trend parameter. When calculating the temporal trend of a single variable, the predictor value of time is not random, and thus the residuals of the regression are used to calculate the effective degrees of freedom, n^* (see, e.g., Smith et al. 2013; Santer et al. 2000), where

$$n^* = n\frac{1-r_1}{1+r_1}. \tag{A1}$$

Here n represents the actual sample size and r_1 is the lag-one autocorrelation of the regression residuals. Whether a trend is significantly different from zero is tested by computing the ratio of the estimated trend, b, and its standard error, s_b (e.g., Santer et al. 2000), which yields

$$t_b = \frac{b}{s_b}, \tag{A2}$$

where t_b is the calculated t value that is then compared to the critical t value for the above stipulated degrees of freedom and significance level.

The statistical significance of the correlation between two independent time series was estimated by testing whether the correlation coefficient, R, between the two detrended time series is significantly different from zero. The calculated value of the Student's t statistic is

$$t = R\sqrt{\frac{n^* - 2}{1 - R^2}}, \tag{A3}$$

with the effective sample size n^* estimated using the relation

$$n^* = n\frac{1 - r_1 r_2}{1 + r_1 r_2}, \tag{A4}$$

where n is the number of samples once again, and r_1, r_2 are the lag-1 autocorrelations for the two time series (Bretherton et al. 1999).

b. *ENSO removal*

Using the monthly mean surface temperature time series (T_s), the ENSO component was removed, as outlined in the main text, by calculating the ''ENSO corrected'' temperatures (T_c) by first determining the optimal lag time in months (L) and the associated regression coefficient (R) between the ENSO index (EI) and T_s, where

$$T_c(t) = T_s(t) - [\mathrm{EI}(t - L)]R. \tag{A5}$$

We found that the optimal ENSO lag signal in the station surface temperature anomalies time was around 3 months. For example, using the monthly mean surface temperatures for the Charleville station from 1950 to 2013, the ENSO regression coefficient for a 3-month lead time was 0.22.

c. *Contributions to long- and short-term SAM variability*

1) Multiple linear regression modeling of SAM

To estimate the relative linkages of ENSO and ozone depletion to both the long-term trend in the summer SAM and its interannual variability, we also performed multiple regressions of the SAM index against sets of different indices representing ENSO, ozone depletion, and other indices similar to the study of Roscoe and Haigh (2007). Two factors of particular interest are the springtime level of ozone depletion and the austral summer ENSO index, which have both been previously shown to be correlated with the summer SAM polarity (L'Heureux and Thompson 2006; Hendon et al. 2007). For each of the ENSO and ozone time series, the slowly varying component was separated from the year-to-year variability by applying a 20-yr low-pass filter (a second-order Butterworth analog filter) to the time series, with reflection of the data values at the beginning and the end of the series. The interannual variability was estimated after removal of the slowly varying component of the time series. In addition to both the short-term (ST; interannual) and long-term (LT) components of ENSO and ozone depletion, we consider the following predictor variables that have been known to perturb temperatures and geopotential heights in the polar stratosphere, and thus have the potential to influence coupling with the tropospheric SAM response (van Loon et al. 2004; Labitzke 2004; Haigh and Roscoe 2006):

1) Quasi-biennial oscillation (QBO). We use the zonal wind at 40 hPa from the compilation of daily wind observations of selected near-equatorial stations provided by the Freie Universität Berlin (http://www.geo.fu-berlin.de/en/met/ag/strat/produkte/qbo/).
2) Solar cycle (Solar). The index used here was based on the 10.7-cm wavelength solar flux measurements provided by the National Research Council of Canada (http://esrl.noaa.gov/psd/data/climateindices/list/#Solar).
3) Stratospheric aerosol optical depth (AOD). The index of tropical (20°S–20°N) AOD was developed by Sato et al. (1993) for use as an external forcing in National Aeronautics and Space Adminsitration (NASA) Goddard Institute for Space Studies (GISS) climate simulations (http://data.giss.nasa.gov/modelforce/strataer/).

To estimate the contributions of the long-term changes in Antarctic ozone and the summertime behavior of ENSO to the long-term change in SAM, we first fit a ''base'' regression model, incorporating five different DJF SAM predictor variables (the QBO, AOD, Solar, ENSO ST, and O_3 ST). In the next step, either the long-term components of changes in November ozone or DJF ENSO were added separately to the base regression model, and the regression models were ranked. We determine the statistical significance of our regression results in two different ways (see below): based on changes in the F test when parameters are added and using the Akaike information criterion (AIC). These results are shown in the top half of Table A1. Over the analysis period used here, inclusion of the slowly varying component of springtime ozone provides a significantly better fit to the DJF SAM than the inclusion of the slowly varying component of the DJF ENSO time series. This is indicated by the larger values of F_{add}, the AIC weights, the regression slope, and the higher statistical significance. We conclude therefore that the long-term trend in the SAM is more strongly linked to

TABLE A1. Regression model results for two different cases: 1) investigating contributions to low-frequency changes in the SAM with common regression indices of QBO, Solar, AOD, ENSO ST, and O_3 ST (Base I); and 2) investigating contributions to interannual variations in the SAM with common regression indices of QBO, Solar, AOD, ENSO LT, and O_3 LT (Base II). The number of variables used in the regression is denoted by m; F_{add} is the improvement in the F test for the addition of a parameter, along with the calculated AIC weights, the regression slope of the added variable, and its significance (estimated using a two-sided Student's t test).

Regression model parameters	m	F_{add}	AIC weights	Reg. slope of added parameter	Significance (%)
Base I	5	—	0.02	—	—
Base I + ENSO LT	6	1.84	0.01	−0.80	81.3
Base I + O_3 LT	6	10.9	0.97	−1.76	**99.7**
Base II	5	—	0.11	—	—
Base II + ENSO ST	6	1.73	0.04	−0.84	79.5
Base II + O_3 ST	6	7.34	0.86	−1.74	**98.9**

the low-frequency changes in stratospheric ozone than to gradual secular changes in the summertime behavior of ENSO.

We use the same method to compare the contributions of the year-to-year variability in November ozone (linked to winter stratospheric wave activity) and summer ENSO behavior, with the results shown in the bottom half of Table A1. Similar to the first case, interannual springtime ozone variability is a larger predictor of the DJF SAM than the interannual variability in the DJF ENSO index. It should be noted that the regression results do not address the potential issue of collinearity between the predictor variables.

2) SIGNIFICANCE OF REGRESSION RESULTS

The amplitudes of the climate variable indices were all scaled to unity prior to the regression analysis, so the regression slope is in the same standardized units of the SAM and the magnitudes of different physical quantities can be compared in a meaningful way. The first method used for identifying the best model of a set of regressions with different predictor variables is to calculate the F statistic for each regression and look at the improvement of the F statistic when an additional predictor variable is added to the base case. Here, the additional predictor variable is either the ENSO index or ozone time series. As in von Storch and Zwiers (2002), the F value is defined as

$$F = \frac{\mathrm{SSR}/n_R}{\mathrm{SSE}/n_E}, \tag{A6}$$

where SSR is the regression sum of squares, n_R is the degrees of freedom for the regression (which here is equal to, m, the number of predictor variables used), SSE is the residual sum of squares, and n_E is the degrees of freedom in the residuals. Here, n_E is equal to $(n - m - 1)$, with n being the sample size of the SAM index. The significance of adding an extra predictor variable to the base regression model can be found from

$$F_{\mathrm{add}} = \frac{\mathrm{SSR(with\ new\ index\ added)} - \mathrm{SSR(base)}}{\mathrm{SSE(with\ new\ index\ added)}/n_E}. \tag{A7}$$

We compare the different F_{add} values that are obtained when summer ENSO and springtime ozone are added separately to the base regression model for the SAM.

The second method of assessing the statistical significance of different regression models relies on the Akaike information criterion. Different regression models are ranked based on their AIC weights (Burnham and Anderson 1998):

$$\mathrm{AIC}_i = n\log(\mathrm{SSE}/n) + 2(m+1), \tag{A8}$$

$$\Delta_i = \mathrm{AIC}_i - 0.5[\min(\mathrm{AIC}_i)], \tag{A9}$$

$$w_i = \frac{e^{-0.5\Delta_i}}{\sum_{r=1}^{r=R} e^{-0.5\Delta_r}}, \tag{A10}$$

where i are the regression models to be compared, and R is the number of alternative models r to be considered. Each AIC weight w_i is the probability that the regression model is the best of the given set of models. Both the F test and AIC weights were used to compare the improvement of the model with the addition of another predictor variable.

d. *Summer daily maximum temperature distributions*

For estimates of the probability distribution functions shown in Fig. 6 of the main text, we used the following steps to partition results for ozone hole and pre–ozone hole periods, and to remove the ENSO influence with the results found in Table A2:

1) Ozone data are available from 1956 to 2013. Partition this period of data availability into a pre–ozone hole era (1956–1984; 28 yr) and the ozone hole era (1985–2013; 29 yr). Since the ozone hole reached its peak depletion in the late 1990s and early 2000s, the use of the years from 1979 to 1985 to define pre– and post–ozone hole

TABLE A2. Results from the Kolmogorov-Smirnov (K-S) and Mann-Whitney (M-W) significance tests applied to distributions of maximum daily temperatures. The total number of measurements (days) used are also provided. The standard deviations are the composite mean values for the individual stations within the region.

Region	Period	Number of days		K-S significance (p value)	M-W significance (p value)	Standard Deviations (°C)
		High	Low			
Australia	1956–84	51 283	43 845	2.6×10^{-002}	2.2×10^{-001}	4.0
	1985–2012	44 488	67 285	$<10^{-100}$	$<10^{-100}$	4.0
Eastern	1956–84	31 693	27 070	2.5×10^{-005}	6.0×10^{-007}	3.7
	1985–2012	27 565	41 601	$<10^{-100}$	$<10^{-100}$	3.7
Southeastern	1956–84	17 715	15 067	6.0×10^{-003}	2.5×10^{-001}	4.5
	1985–2012	15 543	23 332	$<10^{-010}$	$<10^{-010}$	4.5
Northern	1956–84	36 613	31 247	4.2×10^{-008}	3.5×10^{-009}	2.9
	1985–2012	31 817	41 601	$<10^{-100}$	$<10^{-100}$	2.9
Southern	1956–84	14 670	12 598	8.6×10^{-004}	7.8×10^{-002}	4.4
	1985–2012	12 671	19 190	$<10^{-010}$	$<10^{-100}$	4.4
Southwestern	1956–84	2501	2149	$<10^{-010}$	1.3×10^{-004}	4.1
	1985–2012	2144	3244	2.6×10^{-005}	2.6×10^{-004}	4.1
Argentina	1956–84	1631	1541	4.3×10^{-003}	1.1×10^{-003}	4.2
	1985–2012	1406	1628	$<10^{-010}$	$<10^{-010}$	3.8
South Africa	1956–84	—	—	—	—	—
	1985–2012	4974	8021	4.6×10^{-002}	1.8×10^{-002}	3.3
Namibia	1956–84	—	—	—		—
	1985–2012	1729	2558	1.3×10^{-007}	3.6×10^{-006}	2.9
Botswana	1956–84	—	—	—	—	—
	1985–2012	1081	1761	$<10^{-010}$	$<10^{-010}$	2.8

eras had little impact on our results. Our definitions of pre– and post–ozone hole periods are similar to those chosen by Manatsa et al. (2013).

2) In each era, we divide years into groups of high and low ozone years. This was done by first linearly detrending the data for each analysis period and then identifying the years in which the anomalies exceeded or fell below a predefined threshold. The threshold was arbitrarily set at 0.8 times one standard deviation. The high years in the pre–ozone hole era are 1957, 1962, 1964, 1968, 1971, 1972, and 1978 and the low ozone years are 1959, 1961, 1965, 1969, 1982, and 1984. For the ozone hole era, the two groups are (respectively) 1986, 1988, 2000, 2002, 2005, 2012 and 1987, 1993, 1995, 1996, 1998, 1999, 2006, 2008, 2011. Our results were found to be robust to the arbitrary threshold used for low and high ozone years (within the range of 0.8 to 1.2 times the temporal standard deviation).
3) Individual maximum daily temperature data from stations that have observations from 1950 through 2013 were obtained from the Australian Bureau of Meteorology, which identifies five climatologically distinct regions: northern (north of 26°S), southern (south of 26°S), southwestern (southwest of the line joining 30°S, 115°E and 35°S, 120°E), southeastern (south of 33°S, east of 135°E), and eastern Australia (Queensland, New South Wales, Victoria, and Tasmania). Maximum daily temperature data from other countries were taken from GHCN data.
4) The ENSO signal was removed from each individual station temperature time series using the lagged regression method described above. The slight modification was that the ENSO variability calculated was for the monthly-mean daily maximum temperatures, which was then removed from all days in the corresponding month.
5) After removal of the ENSO signal from each station's surface temperature data, the summer months (DJF) were extracted for the pre–ozone hole and ozone hole eras. The anomalies were normalized by the standard deviation, σ, with respect to the era. Next, the high and low ozone years were extracted and regional-average temperatures were calculated. Probability distribution functions (PDFs) for the high and low years were computed. The partitioning (between high and low ozone years) was done for both the original surface temperature data and the dataset with ENSO removed.
6) The PDFs were estimated using a rectangular kernel density function with only weak smoothing in order to preserve the underlying histogram shape.
7) We used both the Kolmogorov–Smirnov (K-S) test and the Mann–Whitney (M-W) test to determine whether there were statistically significant differences between two PDFs. Both are nonparametric tests of the null hypothesis that the two distributions are similar. The M-W test ranks all the distribution values, and then computes a p value that depends on

the discrepancy between the mean ranks of the two groups, while the K-S test compares the cumulative distribution of the two datasets, and computes a *p* value that depends on the largest discrepancy between distributions. The K-S test is sensitive to any differences in the two distributions (differences in shape, spread, or median) whereas the M-W test is mostly sensitive to changes in the median.

REFERENCES

Adler, R. F., and Coauthors, 2003: The version-2 Global Precipitation Climatology Project (GPCP) monthly precipitation analysis (1979–present). *J. Hydrometeor.,* **4,** 1147–1167, doi:10.1175/1525-7541(2003)004<1147:TVGPCP>2.0.CO;2.

Anderson, J., 1979: Impacts of climatic variability in Australian agriculture: A review. *Rev. Mark. Agric. Econ.,* **47,** 147–177.

Andrews, D., J. Holton, and C. Leovy, 1987: *Middle Atmosphere Dynamics.* Academic Press, 489 pp.

Archer, C. L., and K. Caldeira, 2008: Historical trends in the jet streams. *Geophys. Res. Lett.,* **35,** L08803, doi:10.1029/2008GL033614.

Bitz, C. M., and L. M. Polvani, 2012: Antarctic climate response to stratospheric ozone depletion in a fine resolution ocean climate model. *Geophys. Res. Lett.,* **39,** L20705, doi:10.1029/2012GL053393.

Bosilovich, M. G., F. R. Robertson, and J. Chen, 2011: Global energy and water budgets in MERRA. *J. Climate,* **24,** 5721–5739, doi:10.1175/2011JCLI4175.1.

Bretherton, C., M. Widmann, V. Dymnikov, J. Wallace, and I. Bladé, 1999: The effective number of spatial degrees of freedom of a time-varying field. *J. Climate,* **12,** 1990–2009, doi:10.1175/1520-0442(1999)012<1990:TENOSD>2.0.CO;2.

Burnham, K. P., and D. R. Anderson, 1998: Akaike's information criterion: 1973. *Model Selection and Inference: A Practical Information-Theoretic Approach,* 2nd ed. Springer Verlag, 60–65.

Cai, W., P. Whetton, and D. Karoly, 2003: The response of the Antarctic Oscillation to increasing and stabilized atmospheric CO_2. *J. Climate,* **16,** 1525–1538, doi:10.1175/1520-0442-16.10.1525.

Chen, G., J. Lu, and D. M. W. Frierson, 2008: Phase speed spectra and the latitude of surface westerlies: Interannual variability and global warming trend. *J. Climate,* **21,** 5942–5959, doi:10.1175/2008JCLI2306.1.

Christiansen, B., 1999: Stratospheric vacillations in a general circulation model. *J. Atmos. Sci.,* **56,** 1858–1872, doi:10.1175/1520-0469(1999)056<1858:SVIAGC>2.0.CO;2.

Dee, D. P., and Coauthors, 2011: The ERA-Interim reanalysis: Configuration and performance of the data assimilation system. *Quart. J. Roy. Meteor. Soc.,* **137,** 553–597, doi:10.1002/qj.828.

Fogt, R. L., J. Perlwitz, A. J. Monaghan, D. H. Bromwich, J. M. Jones, and G. J. Marshall, 2009a: Historical SAM variability. Part II: Twentieth-century variability and trends from reconstructions, observations, and the IPCC AR4 models. *J. Climate,* **22,** 5346–5365, doi:10.1175/2009JCLI2786.1.

——, ——, S. Pawson, and M. A. Olsen, 2009b: Intra-annual relationships between polar ozone and the SAM. *Geophys. Res. Lett.,* **36,** L04707, doi:10.1029/2008GL036627.

Fyfe, J. C., G. J. Boer, and G. M. Flato, 1999: The Arctic and Antarctic oscillations and their projected changes under global warming. *Geophys. Res. Lett.,* **26,** 1601–1604, doi:10.1029/1999GL900317.

——, O. Saenko, K. Zickfeld, M. Eby, and A. Weaver, 2007: The role of poleward-intensifying winds on Southern Ocean warming. *J. Climate,* **20,** 5391–5400, doi:10.1175/2007JCLI1764.1.

——, N. P. Gillett, and G. J. Marshall, 2012: Human influence on extratropical Southern Hemisphere summer precipitation. *Geophys. Res. Lett.,* **39,** L23711, doi:10.1029/2012GL054199.

Gerber, E. P., and Coauthors, 2012: Assessing and understanding the impact of stratospheric dynamics and variability on the Earth system. *Bull. Amer. Meteor. Soc.,* **93,** 845–859, doi:10.1175/BAMS-D-11-00145.1.

Gillett, N. P., and D. W. J. Thompson, 2003: Simulation of recent Southern Hemisphere climate change. *Science,* **302,** 273–275, doi:10.1126/science.1087440.

——, T. D. Kell, and P. D. Jones, 2006: Regional climate impacts of the southern annular mode. *Geophys. Res. Lett.,* **33,** L23704, doi:10.1029/2006GL027721.

Gong, D., and S. Wang, 1999: Definition of Antarctic oscillation index. *Geophys. Res. Lett.,* **26,** 459–462, doi:10.1029/1999GL900003.

Gonzalez, P. L. M., L. M. Polvani, R. Seager, and G. J. P. Correa, 2014: Stratospheric ozone depletion: A key driver of recent precipitation trends in south eastern South America. *Climate Dyn.,* **42,** 1775–1792, doi:10.1007/s00382-013-1777-x.

Grise, K. M., D. W. J. Thompson, and P. M. Forster, 2009: On the role of radiative processes in stratosphere–troposphere coupling. *J. Climate,* **22,** 4154–4161, doi:10.1175/2009JCLI2756.1.

Gunasekera, D., C. Tulloh, M. Ford, and E. Heyhoe, 2008: Climate change: Opportunities and challenges in Australian agriculture. *Proc. Faculty of Agriculture, Food and Natural Resources Annual Symp.,* Sydney, NSW, Australia, University of Sydney, p.5.

Haigh, J. D., and H. K. Roscoe, 2006: Solar influences on polar modes of variability. *Meteor. Z.,* **15,** 371–378, doi:10.1127/0941-2948/2006/0123.

——, and ——, 2009: The final warming date of the Antarctic polar vortex and influences on its interannual variability. *J. Climate,* **22,** 5809–5819, doi:10.1175/2009JCLI2865.1.

Hartmann, D. L., and F. Lo, 1998: Wave-driven zonal flow vacillation in the Southern Hemisphere. *J. Atmos. Sci.,* **55,** 1303–1315, doi:10.1175/1520-0469(1998)055<1303:WDZFVI>2.0.CO;2.

——, J. M. Wallace, V. Limpasuvan, D. W. Thompson, and J. R. Holton, 2000: Can ozone depletion and global warming interact to produce rapid climate change? *Proc. Natl. Acad. Sci. USA,* **97,** 1412–1417, doi:10.1073/pnas.97.4.1412.

Haynes, P., M. McIntyre, T. G. Shepherd, C. J. Marks, and K. P. Shine, 1991: On the downward control of extratropical diabatic circulations by eddy-induced mean zonal forces. *J. Atmos. Sci.,* **48,** 651–678, doi:10.1175/1520-0469(1991)048<0651:OTCOED>2.0.CO;2.

Hendon, H. H., D. W. J. Thompson, and M. C. Wheeler, 2007: Australian rainfall and surface temperature variations associated with the Southern Hemisphere annular mode. *J. Climate,* **20,** 2452–2467, doi:10.1175/JCLI4134.1.

Hennessy, K., and A. Pittock, 1995: Greenhouse warming and threshold temperature events in Victoria, Australia. *Int. J. Climatol.,* **15,** 591–612, doi:10.1002/joc.3370150602.

Hu, Y., and Q. Fu, 2007: Observed poleward expansion of the Hadley circulation since 1979. *Atmos. Chem. Phys. Discuss.,* **7,** 9367–9384, doi:10.5194/acpd-7-9367-2007.

Hurrell, J., and H. Van Loon, 1994: A modulation of the atmospheric annual cycle in the Southern Hemisphere. *Tellus,* **46A,** 325–338, doi:10.1034/j.1600-0870.1994.t01-1-00007.x.

Jones, J. M., and M. Widmann, 2003: Instrument and tree-ring-based estimates of the Antarctic Oscillation. *J. Climate,* **16,** 3511–3524, doi:10.1175/1520-0442(2003)016<3511:IATEOT>2.0.CO;2.

Joshi, M. M., J. M. Gregory, M. J. Webb, D. M. H. Sexton, and T. C. Johns, 2008: Mechanisms for the land/sea warming contrast exhibited by simulations of climate change. *Climate Dyn.,* **30,** 455–465, doi:10.1007/s00382-007-0306-1.

Kang, S. M., L. M. Polvani, J. C. Fyfe, and M. Sigmond, 2011: Impact of polar ozone depletion on subtropical precipitation. *Science,* **332,** 951–954, doi:10.1126/science.1202131.

——, ——, ——, S.-W. Son, M. Sigmond, and G. J. P. Correa, 2013: Modeling evidence that ozone depletion has impacted extreme precipitation in the austral summer. *Geophys. Res. Lett.,* **40,** 4054–4059, doi:10.1002/grl.50769.

Karoly, D., 1989: Southern Hemisphere circulation features associated with El Niño–Southern Oscillation events. *J. Climate,* **2,** 1239–1252, doi:10.1175/1520-0442(1989)002<1239:SHCFAW>2.0.CO;2.

——, 1990: The role of transient eddies in low-frequency zonal variations of the Southern Hemisphere circulation. *Tellus,* **42A,** 41–50, doi:10.1034/j.1600-0870.1990.00005.x.

——, and Q. Wu, 2005: Detection of regional surface temperature trends. *J. Climate,* **18,** 4337–4344, doi:10.1175/JCLI3565.1.

——, P. Hope, and P. Jones, 1996: Decadal variations of the Southern Hemisphere circulation. *Int. J. Climatol.,* **16,** 723–738, doi:10.1002/(SICI)1097-0088(199607)16:7<723::AID-JOC54>3.0.CO;2-6.

Karpechko, A., N. P. Gillett, G. J. Marshall, and A. Scaife, 2008: Stratospheric influence on circulation changes in the Southern Hemisphere troposphere in coupled climate models. *Geophys. Res. Lett.,* **35,** L20806, doi:10.1029/2008GL035354.

Kidson, J., 1988: Interannual variations in the Southern Hemisphere circulation. *J. Climate,* **1,** 1177–1198, doi:10.1175/1520-0442(1988)001<1177:IVITSH>2.0.CO;2.

Kushner, P., and L. Polvani, 2004: Stratosphere–troposphere coupling in a relatively simple AGCM: The role of eddies. *J. Climate,* **17,** 629–639, doi:10.1175/1520-0442(2004)017<0629:SCIARS>2.0.CO;2.

——, I. Held, and T. Delworth, 2001: Southern Hemisphere atmospheric circulation response to global warming. *J. Climate,* **14,** 2238–2249, doi:10.1175/1520-0442(2001)014<0001:SHACRT>2.0.CO;2.

Labitzke, K., 2004: On the signal of the 11-year sunspot cycle in the stratosphere over the Antarctic and its modulation by the Quasi-Biennial Oscillation (QBO). *Meteor. Z.,* **13,** 263–270, doi:10.1127/0941-2948/2004/0013-0263.

Lawrimore, J. H., M. J. Menne, B. E. Gleason, C. N. Williams, D. B. Wuertz, R. S. Vose, and J. Rennie, 2011: An overview of the Global Historical Climatology Network monthly mean temperature data set, version 3. *J. Geophys. Res.,* **116,** D19121, doi:10.1029/2011JD016187.

Lee, S., and S. B. Feldstein, 2013: Detecting ozone and greenhouse gas–driven wind trends with observational data. *Science,* **339,** 563–567, doi:10.1126/science.1225154.

Lehmann, E. L., 2006: *Nonparametrics: Statistical Methods Based on Ranks.* 2nd ed. Springer, 464 pp.

Lewis, S. C., and D. J. Karoly, 2013: Anthropogenic contributions to Australia's record summer temperatures of 2013. *Geophys. Res. Lett.,* **40,** 3705–3709, doi:10.1002/grl.50673.

L'Heureux, M., and D. Thompson, 2006: Observed relationships between the El Niño–Southern Oscillation and the extratropical zonal-mean circulation. *J. Climate,* **19,** 276–287, doi:10.1175/JCLI3617.1.

Li, F., P. Newman, and R. S. Stolarski, 2010: Relationships between the Brewer–Dobson circulation and the southern annular mode during austral summer in coupled chemistry–climate model simulations. *J. Geophys. Res.,* **115,** D15106, doi:10.1029/2009JD012876.

Livezey, R., and W. Chen, 1983: Statistical field significance and its determination by Monte Carlo techniques. *Mon. Wea. Rev.,* **111,** 46–59, doi:10.1175/1520-0493(1983)111<0046:SFSAID>2.0.CO;2.

Lu, J., G. Chen, and D. M. W. Frierson, 2008: Response of the zonal mean atmospheric circulation to El Niño versus global warming. *J. Climate,* **21,** 5835–5851, doi:10.1175/2008JCLI2200.1.

Manatsa, D., Y. Morioka, S. K. Behera, T. Yamagata, and C. H. Matarira, 2013: Link between Antarctic ozone depletion and summer warming over southern Africa. *Nat. Geosci.,* **6,** 934–939, doi:10.1038/ngeo1968.

Marshall, G., 2003: Trends in the southern annular mode from observations and reanalyses. *J. Climate,* **16,** 4134–4143, doi:10.1175/1520-0442(2003)016<4134:TITSAM>2.0.CO;2.

——, 2007: Half-century seasonal relationships between the southern annular mode and Antarctic temperatures. *Int. J. Climatol.,* **27,** 373–383, doi:10.1002/joc.1407.

Marshall, J., A. Donohoe, D. Ferreira, and D. McGee, 2014: The ocean's role in setting the mean position of the Inter-Tropical Convergence Zone. *Climate Dyn.,* **42,** 1967-1979, doi:10.1007/s00382-013-1767-z.

Matsuno, T., 1971: A dynamical model of the stratospheric sudden warming. *J. Atmos. Sci.,* **28,** 1479–1494, doi:10.1175/1520-0469(1971)028<1479:ADMOTS>2.0.CO;2.

Meneghini, B., 2007: Association between Australian rainfall and the southern annular mode. *Int. J. Climatol.,* **27,** 109–121, doi:10.1002/joc.1370.

Orr, A., D. Cresswell, G. J. Marshall, J. C. R. Hunt, J. Sommeria, C. G. Wang, and M. Light, 2004: A low-level explanation for the recent large warming trend over the western Antarctic Peninsula involving blocked winds and changes in zonal circulation. *Geophys. Res. Lett.,* **31,** L06204, doi:10.1029/2003GL019160.

——, T. J. Bracegirdle, J. S. Hosking, T. Jung, J. D. Haigh, T. Phillips, and W. Feng, 2012: Possible dynamical mechanisms for Southern Hemisphere climate change due to the ozone hole. *J. Atmos. Sci.,* **69,** 2917–2932, doi:10.1175/JAS-D-11-0210.1.

Papoulis, A., 1990: *Probability and Statistics.* Prentice Hall, 512 pp.

Perlwitz, J., S. Pawson, R. L. Fogt, J. E. Nielsen, and W. D. Neff, 2008: Impact of stratospheric ozone hole recovery on Antarctic climate. *Geophys. Res. Lett.,* **35,** L08714, doi:10.1029/2008GL033317.

Polvani, L. M., and D. W. Waugh, 2004: Upward wave activity flux as a precursor to extreme stratospheric events and subsequent anomalous surface weather regimes. *J. Climate,* **17,** 3548–3555, doi:10.1175/1520-0442(2004)017<3548:UWAFAA>2.0.CO;2.

——, ——, G. J. P. Correa, and S.-W. Son, 2011: Stratospheric ozone depletion: The main driver of twentieth-century atmospheric circulation changes in the Southern Hemisphere. *J. Climate,* **24,** 795–812, doi:10.1175/2010JCLI3772.1.

Randel, W. J., and Coauthors, 2009: An update of observed stratospheric temperature trends. *J. Geophys. Res.,* **114,** D02107, doi:10.1029/2008JD010421.

Rauthe, M., and H. Paeth, 2004: Relative importance of Northern Hemisphere circulation modes in predicting regional climate change. *J. Climate,* **17,** 4180–4189, doi:10.1175/JCLI3140.1.

Rienecker, M. M., and Coauthors, 2011: MERRA: NASA's Modern-Era Retrospective Analysis for Research and Applications. *J. Climate,* **24,** 3624–3648, doi:10.1175/JCLI-D-11-00015.1.

Roscoe, H. K, and J. D. Haigh, 2007: Influences of ozone depletion, the solar cycle and the QBO on the southern annular mode. *Quart. J. Roy. Meteor. Soc.,* **133,** 1855–1864, doi:10.1002/qj.153.

Roscoe, H. K., G. J. Marshall, and J. C. King, 2006: Low potential for stratospheric dynamical change to be implicated in the large winter warming in the central Antarctic Peninsula. *Quart. J. Roy. Meteor. Soc.,* **132,** 803–820, doi:10.1256/qj.05.81.

Salby, M., 2008: Involvement of the Brewer–Dobson circulation in changes of Northern Hemisphere ozone. *Dyn. Atmos. Oceans,* **44,** 143–164, doi:10.1016/j.dynatmoce.2006.11.002.

Santer, B. D., J. J. Hnilo, T. M. L. Wigley, J. S. Boyle, C. Doutriaux, M. Fiorino, D. E. Parker, and K. E. Taylor, 1999: Uncertainties in observationally based estimates of temperature change in the free atmosphere. *J. Geophys. Res.,* **104** (D6), 6305–6333, doi:10.1029/1998JD200096.

——, T. M. L. Wigley, J. Boyle, D. J. Gaffen, J. Hnilo, D. Nychka, D. Parker, and K. Taylor, 2000: Statistical significance of trends and trend differences in layer-average atmospheric temperature time series. *J. Geophys. Res.,* **105** (D6), 7337–7356, doi:10.1029/1999JD901105.

Sato, M., J. Hansen, M. McCormick, and J. Pollack, 1993: Stratospheric aerosol optical depths, 1850–1990. *J. Geophys. Res.,* **98** (D12), 22 987–22 994, doi:10.1029/93JD02553.

Schneider, D. P., C. Deser, and Y. Okumura, 2012: An assessment and interpretation of the observed warming of West Antarctica in the austral spring. *Climate Dyn.,* **38,** 323–347, doi:10.1007/s00382-010-0985-x.

Schoeberl, M. R., and D. L. Hartmann, 1991: The dynamics of the stratospheric polar vortex and its relation to springtime ozone depletions. *Science,* **251,** 46–52, doi:10.1126/science.251.4989.46.

Screen, J. A., N. P. Gillett, D. P. Stevens, G. J. Marshall, and H. K. Roscoe, 2009: The role of eddies in the Southern Ocean temperature response to the southern annular mode. *J. Climate,* **22,** 806–818, doi:10.1175/2008JCLI2416.1.

Seager, R., N. Harnik, and Y. Kushnir, 2003: Mechanisms of hemispherically symmetric climate variability. *J. Climate,* **16,** 2960–2978, doi:10.1175/1520-0442(2003)016<2960:MOHSCV>2.0.CO;2.

Sen Gupta, A., and M. England, 2006: Coupled ocean–atmosphere–ice response to variations in the southern annular mode. *J. Climate,* **19,** 4457–4486, doi:10.1175/JCLI3843.1.

Shaw, T. A., J. Perlwitz, N. Harnik, P. A. Newman, and S. Pawson, 2011: The impact of stratospheric ozone changes on downward wave coupling in the Southern Hemisphere. *J. Climate,* **24,** 4210–4229, doi:10.1175/2011JCLI4170.1.

Shindell, D. T., and G. A. Schmidt, 2004: Southern Hemisphere climate response to ozone changes and greenhouse gas increases. *Geophys. Res. Lett.,* **31,** L18209, doi:10.1029/2004GL020724.

——, S. Wong, and D. Rind, 1997: Interannual variability of the Antarctic ozone hole in a GCM. Part I: The influence of tropospheric wave variability. *J. Atmos. Sci.,* **54,** 2308–2319, doi:10.1175/1520-0469(1997)054<2308:IVOTAO>2.0.CO;2.

Sigmond, M., J. C. Fyfe, and J. F. Scinocca, 2010: Does the ocean impact the atmospheric response to stratospheric ozone depletion? *Geophys. Res. Lett.,* **37,** L12706, doi:10.1029/2010GL043773.

Smith, K. L., L. M. Polvani, and D. R. Marsh, 2012: Mitigation of 21st century Antarctic sea ice loss by stratospheric ozone recovery. *Geophys. Res. Lett.,* **39,** L20701, doi:10.1029/2012GL053325.

Smith, R., S. Stammerjohn, and K. Baker, 2013: Surface air temperature variations in the Western Antarctic Peninsula region. *Foundations for Ecological Research West of the Antarctic Peninsula,* R. Ross, E. Hofmann, and L. Quetin, Eds., Antartcic Research Series, Vol. 70, American Geophysical Union, 105–121.

Solomon, S., 1999: Stratospheric ozone depletion: A review of concepts and history. *Rev. Geophys.,* **37,** 275–316, doi:10.1029/1999RG900008.

Son, S.-W., A. Purich, H. H. Hendon, B.-M. Kim, and L. Polvani, 2013: Improved seasonal forecast using ozone hole variability? *Geophys. Res. Lett.,* **40,** 6231–6235, doi:10.1002/2013GL057731.

Song, Y., and W. Robinson, 2004: Dynamical mechanisms for stratospheric influences on the troposphere. *J. Atmos. Sci.,* **61,** 1711–1725, doi:10.1175/1520-0469(2004)061<1711:DMFSIO>2.0.CO;2.

Stone, D., A. Weaver, and R. Stouffer, 2001: Projection of climate change onto modes of atmospheric variability. *J. Climate,* **14,** 3551–3565, doi:10.1175/1520-0442(2001)014<3551:POCCOM>2.0.CO;2.

Suppiah, R., D. Collins, and P. Della-Marta, 2001: Observed changes in Australian climate. Bureau of Meteorology and CSIRO Division of Atmospheric Research Tech. Rep., 6 pp. [Available online at http://www.cmar.csiro.au/e-print/open/suppiah_2001a.pdf.]

Thompson, D. W. J., and J. M. Wallace, 2000: Annular modes in the extratropical circulation. Part I: Month-to-month variability. *J. Climate,* **13,** 1000–1016, doi:10.1175/1520-0442(2000)013<1000:AMITEC>2.0.CO;2.

——, and ——, 2001: Regional climate impacts of the Northern Hemisphere annular mode. *Science,* **293,** 85–89, doi:10.1126/science.1058958.

——, and S. Solomon, 2002: Interpretation of recent Southern Hemisphere climate change. *Science,* **296,** 895–899, doi:10.1126/science.1069270.

——, M. P. Baldwin, and S. Solomon, 2005: Stratosphere–troposphere coupling in the Southern Hemisphere. *J. Atmos. Sci.,* **62,** 708–715, doi:10.1175/JAS-3321.1.

——, J. C. Furtado, and T. G. Shepherd, 2006: On the tropospheric response to anomalous stratospheric wave drag and radiative heating. *J. Atmos. Sci.,* **63,** 2616–2629, doi:10.1175/JAS3771.1.

——, S. Solomon, P. J. Kushner, M. H. England, K. M. Grise, and D. J. Karoly, 2011: Signatures of the Antarctic ozone hole in Southern Hemisphere surface climate change. *Nat. Geosci.,* **4,** 741–749, doi:10.1038/ngeo1296.

Thorne, P. W., 2005: Revisiting radiosonde upper air temperatures from 1958 to 2002. *J. Geophys. Res.,* **110,** D18105, doi:10.1029/2004JD005753.

Trenberth, K. E., 1984: Some effects of finite sample size and persistence on meteorological statistics. Part I: Autocorrelations. *Mon. Wea. Rev.,* **112,** 2359–2368, doi:10.1175/1520-0493(1984)112<2359:SEOFSS>2.0.CO;2.

——, J. T. Fasullo, and J. Mackaro, 2011: Atmospheric moisture transports from ocean to land and global energy flows in reanalyses. *J. Climate,* **24,** 4907–4924, doi:10.1175/2011JCLI4171.1.

Trewin, B., 2013: A daily homogenized temperature data set for Australia. *Int. J. Climatol.,* **33,** 1510–1529, doi:10.1002/joc.3530.

Turner, J., and Coauthors, 2004: The SCAR READER Project: Toward a high-quality database of mean Antarctic meteorological observations. *J. Climate,* **17,** 2890–2898, doi:10.1175/1520-0442(2004)017<2890:TSRPTA>2.0.CO;2.

van Loon, H., G. A. Meehl, and J. M. Arblaster, 2004: A decadal solar effect in the tropics in July–August. *J. Atmos. Sol.-Terr. Phys.,* **66,** 1767–1778, doi:10.1016/j.jastp.2004.06.003.

von Storch, H., and F. W. Zwiers, 2002: *Statistical Analysis in Climate Research.* Cambridge University Press, 496 pp.

Watterson, I., 2000: Southern midlatitude zonal wind vacillation and its interaction with the ocean in GCM simulations. *J. Climate,* **13,** 562–578, doi:10.1175/1520-0442(2000)013<0562:SMZWVA>2.0.CO;2.

Waugh, D., and W. Randel, 1999: Climatology of Arctic and Antarctic polar vortices using elliptical diagnostics. *J. Atmos. Sci.,* **56,** 1594–1613, doi:10.1175/1520-0469(1999)056<1594:COAAAP>2.0.CO;2.

Weber, M., S. Dikty, J. P. Burrows, H. Garny, M. Dameris, A. Kubin, J. Abalichin, and U. Langematz, 2011: The Brewer-Dobson circulation and total ozone from seasonal to decadal time scales. *Atmos. Chem. Phys.,* **11,** 11 221–11 235, doi:10.5194/acp-11-11221-2011.

Welbergen, J. A., S. M. Klose, N. Markus, and P. Eby, 2008: Climate change and the effects of temperature extremes on Australian flying-foxes. *Proc. Biol. Sci.,* **275,** 419–425, doi:10.1098/rspb.2007.1385.

Whetton, P., A. Fowler, M. Haylock, and A. Pittock, 1993: Implications of climate change due to the enhanced greenhouse effect on floods and droughts in Australia. *Climatic Change,* **25,** 289–317, doi:10.1007/BF01098378.

Zhou, S., M. E. Gelman, A. J. Miller, and J. P. McCormack, 2000: An inter-hemisphere comparison of the persistent stratospheric polar vortex. *Geophys. Res. Lett.,* **27,** 1123–1126, doi:10.1029/1999GL011018.